LA-UR-15-21398 (Accepted Manuscript)

Microstructure effects on the recrystallization of low-symmetry alpha-uranium

Mccabe, Rodney James
Richards, Andrew Walter
Coughlin, Daniel Robert
Clarke, Kester Diederik
Beyerlein, Irene Jane
Knezevic, Marko

To be published in: Journal of Nuclear Materials

DOI to publisher's version: 10.1016/j.jnucmat.2015.04.055

Permalink to record: http://permalink.lanl.gov/object/view?what=info:lanl-repo/lareport/LA-UR-15-21398

Microstructure effects on the recrystallization of low-symmetry alpha-uranium

R. J. McCabe[1], A.W. Richards[1], D. Coughlin[1], K.D. Clarke[1], I.J. Beyerlein[2], and M. Knezevic[3]

1. Materials Science and Technology Division, Los Alamos National Laboratory, Los Alamos, NM USA.

2. Theoretical Division, Los Alamos National Laboratory, Los Alamos, NM USA.

3. Dept. of Mech. Eng., U. of New Hampshire, Durham, NH USA

Corresponding Author: R. J. McCabe, MS G770, PO Box 1663, Los Alamos, NM 87545

Abstract

We employ electron backscatter diffraction (EBSD) to investigate microstructural evolution of uranium during recrystallization. To understand the relationship between microstructure and recrystallization, we use measures of intra-granular misorientation within grains and near grain boundaries in both deformed (non-recrystallized) uranium and recrystallizing uranium. The data show that the level of intra-granular misorientation depends on crystallographic orientation. However, contrary to expectation, this relationship does not significantly affect the recrystallization texture. Rather, the analysis suggests that recrystallization nucleation occurs along high angle grain boundaries in the deformed microstructure. Specifically, we show that the nucleation of recrystallized grains correlates well with the spatially heterogeneous distribution of high angle boundaries. Due to the inhomogeneous distribution of high angle boundaries, the recrystallized microstructure after long times exhibits clustered distributions of

small and large grains. Finally, twin boundaries do not appear to act as recrystallization nucleation sites.

Introduction

Similar to the processing of other metals, uranium components are commonly made by a series of mechanical and thermal processes. Mechanical processes such as forging, rolling, swaging, and forming are used to refine the starting cast microstructure and make metal forms for further processing to produce final parts. Thermal annealing processes are interspersed within the mechanical processes to produce finer, recrystallized grains and to soften and restore ductility [1] to a metal for further mechanical processing. The combination of mechanical and thermal processes has significant effects on the evolving microstructures; i.e. grain size, grain morphology, and texture. Significant progress has been made in understanding the microstructure evolution that accompanies deformation of uranium [2-6]. However, little work has been done to understand the recrystallization behavior of uranium [7].

There is a large body of work examining the recrystallization behavior of other metals. The physics, phenomenology, and modeling of recrystallization is well documented in several review articles [1, 8-11]. A vast majority of recrystallization work to date examines recrystallization in metals with face centered cubic (FCC) crystal structures. The recrystallization of body centered cubic (BCC) metals has also received considerable attention, and limited efforts have looked at the recrystallization behavior of hexagonal close packed (HCP) metals [12-15].

One principal aim of the aforementioned body of work is to relate the deformed microstructure to the recrystallized microstructure under subsequent annealing. As defined by [1], "recrystallization is the formation of a new grain structure in a deformed material by the formation and migration of high angle grain boundaries driven by the stored energy of deformation." Over the years, several specific characteristics relating deformed and recrystallized microstructures have been shown. Recrystallization nuclei already exist in the deformed microstructure; i.e., recrystallized grains grow from orientations that are present, although they may not represent dominant deformation orientations in the deformed microstructure [1, 8-9]. Because recrystallization occurs through the motion of high angle grain boundaries, recrystallization nuclei are expected to be in close proximity to the high angle boundaries in the deformed microstructure [8-9]. Grain boundary character[16-17] has also been shown to influence grain boundary mobility, and thus, the rate of growth of nucleating grains [9-10]. In some metals, grain boundaries with certain character are more mobile and this dependence can have a significant influence on the evolving, recrystallizing microstructure. The driving force for recrystallization is the stored energy of deformation, primarily in the form of dislocations [9-10]. The driving force for recrystallization is expected to be higher in grains or regions of high dislocation content. A successful recrystallization nucleus is also expected to have an energetic advantage [10] in addition to sharing a high energy boundary. Finally, the recrystallized grain size depends on the grain size prior to deformation and the amount of deformation applied to the material [9, 18].

As stated previously, many of the above relationships have been reported for deformed metals with cubic crystal structures. Recrystallization of deformed metals with crystal structures of lesser symmetry, such as orthorhombic uranium, has not received nearly as much attention and is comparatively less well understood. These metals deform via several modes of slip and twinning and the relative amounts of these modes are highly sensitive to grain orientation. Thus, interesting and potentially distinct relationships between orientation and the propensity to recrystallize could arise. In the present study, we use electron backscatter diffraction (EBSD) to statistically analyze the relationship between a few important microstructural characteristics to recrystallization in deformed uranium. EBSD is an excellent tool for this study allowing for statistically relevant comparisons of spatially correlated orientation information. In particular, with EBSD it is possible to partition recrystallized grains from the deformed microstructure [7]. Taking advantage of this capability, we show that the development of intra-granular misorientations depends on grain orientation. Interestingly, this relationship has an insignificant effect on recrystallization texture. Our analysis suggests that recrystallization nucleation occurs along high angle grain boundaries in the deformed microstructure, which does affect the evolving texture. In contrast, the twin boundaries do not appear to act as recrystallization nucleation sites.

Experimental

The processing and experimental methods are nearly identical to those reported previously [7]. The previous study was one of the first successful uses of EBSD on uranium, and showed that recrystallized grains can be distinguished from

non-recrystallized grains. A brief discussion of the manufacturing and specimen preparation is given here with details provided in [7]. The present study is based almost entirely on new EBSD data. Any experimental differences from the prior study and distinguishing details of the EBSD analysis will be highlighted.

A series of processing steps were used to produce a uranium plate including vacuum induction casting, hot upset forging (625 °C), and warm clock-rolling. The clock-rolling was performed at 300 °C in eight equivalent strain passes with rotations of 0°, 90°, 135°, 225°, 270°, 360°, 45° and 135° resulting in a final reduction of approximately 50%. The warm-rolling temperature is considerably below temperatures for which recrystallization is observed in rolled uranium for similar levels of deformation, and dynamic recrystallization is not expected for this processing. Isothermal annealing experiments were performed in a quench dilatometer on 3.173 mm diameter, 10 mm long cylindrical samples with the axis of the sample along a consistent in-plane plate direction. Annealing experiments were performed for various times at 435 °C, 450 °C, and 475 °C under a vacuum of 10^{-5} Torr with a heating rate of 7.5 °C/s and quench rate of 10 °C/s to room temperature.

Axial sections cut from near the centers of the dilatometer samples were mounted and metallographically prepared. The EBSD preparation technique consists of polishing to a 1 μm diamond finish followed by two electropolishing steps. The first electropolishing step uses a room temperature, stirred solution of 45% ethanol, 27% ethylene glycol, and 27% phosphoric acid at 10V for around 4

minutes. The second electropolishing step uses a room temperature solution of 5% phosphoric acid and 95% water at 5V for 1-2 s.

Automated EBSD scans were performed at 25 kV in an FEI XL30 SEM equipped with TSL/EDAX data acquisition software. Regions 300 μm by 600 μm roughly at the center of the 3.175 mm diameter mounted specimens were scanned with a step size of 0.5 μm for microstructure analysis. In addition to the microstructure scans, the entire surfaces of the samples were scanned using a step size of 5 μm to generate "macro" textures. The orientation data was analyzed using TSL/EDAX Orientation Imaging Microscopy (OIM) Analysis 7.2 software. A minimal EBSD clean-up was performed on each of the microstructure scans using a neighbor confidence index correlation with a minimum confidence index of 10% of the average for the scan. Because samples were cut from round cross-sections, a priori alignment of samples in the microscope with a consistent orientation relative to the plate normal direction was not possible. Thus, in some maps, deformed grains are elongated vertically (Figure 1a), and in other maps deformed grains are elongated horizontally (Figure 1c) or at arbitrary angles. Texture symmetries are used for orientation alignments with observed grain shapes used for validation.

Results

We use EBSD to relate the deformed microstructure to recrystallization phenomena. Figure 1 shows EBSD orientation maps of samples heat treated for different amounts of time at 450°C. With these data, we quantitatively compare the characteristics of the as-deformed and recrystallizing microstructures. We pay special attention to local and grain level misorientation and characteristics of high-

angle grain boundaries. These choices are based on the assumptions that 1) measures of misorientation correlate with the local defect densities that are expected to serve as a driving force for recrystallization and 2) the motion of high angle boundaries are the mechanism for recrystallization.

To this end, it is necessary to identify in EBSD a recrystallized grain from a non-recrystallized one. Partitioning the recrystallized grains from the non-recrystallized grains allows us to directly measure the recrystallized fraction as a function of time and temperature. As with previous studies [7, 19], it is found that measures of internal grain misorientation work remarkably well for partitioning (separating) recrystallized grains from non-recrystallized grains. This is consistent with previous observations and theories of recrystallization where new, relatively defect-free grains form at the expense of non-recrystallized grains that contain large densities of dislocations. These higher dislocation densities result in higher levels of

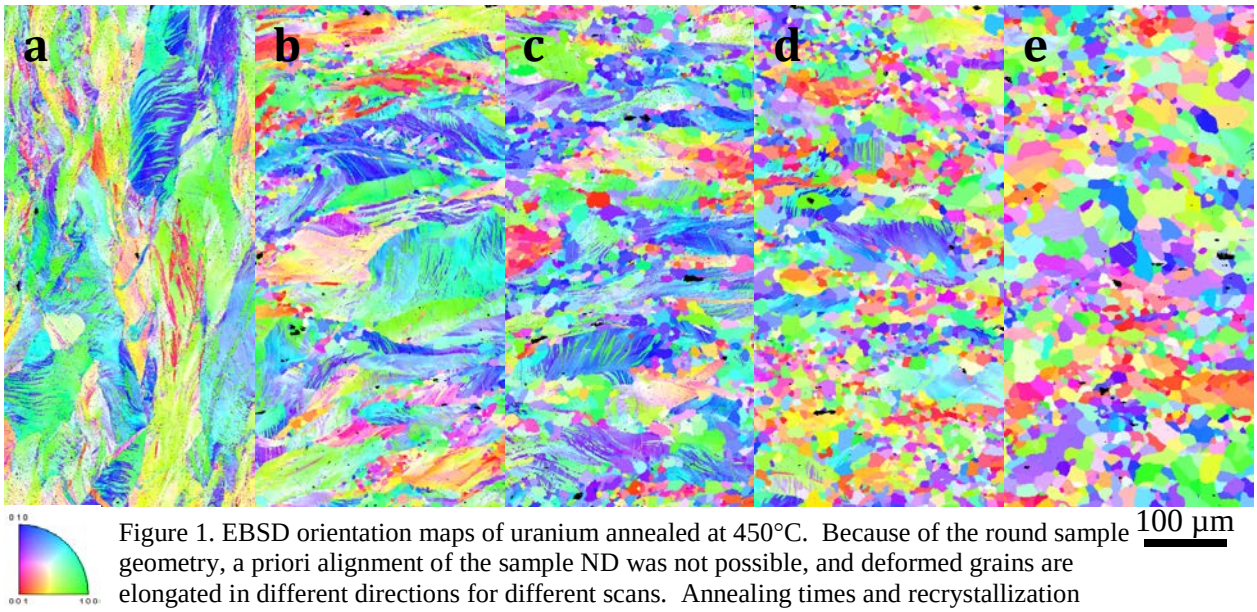

Figure 1. EBSD orientation maps of uranium annealed at 450°C. Because of the round sample geometry, a priori alignment of the sample ND was not possible, and deformed grains are elongated in different directions for different scans. Annealing times and recrystallization fractions a) 30 s - Rx < 1%, b) 600 s - Rx 18%, c) 1800 s – Rx 46%, d) 6000 s – Rx 71%, e) 10^5 s – Rx 91%. Crystal orientations shown are along the final rolling direction.

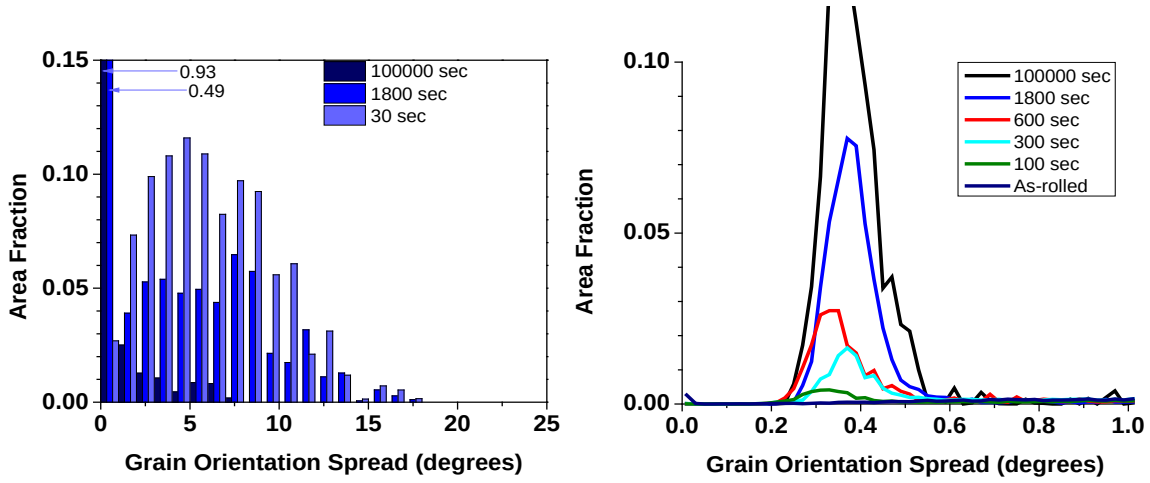

Figure 2. Grain orientation spread (GOS) distributions as a function of annealing time at 450°C. a) The full distribution showing a depletion of high GOS grains accompanying recrystallization. b) GOS distribution below 1° showing the emergence of a new peak accompanying recrystallization

internal grain misorientation.

One measure we use is the Grain Orientation Spread (GOS). GOS is the average deviation between the orientation of each scan point in a given grain and the average grain orientation. Figure2a shows the evolution of the full distribution of measured GOS using a 1° bin size, and Figure2b shows the distribution for GOS less than 1° using a bin size of 0.02°, both for annealing at 450°C. For these plots, a grain tolerance angle of 5° is assumed and deformation twins are assumed to constitute their own grains.

A new peak forms in the GOS distribution between 0.1° and 0.65° as recrystallization occurs. Because of the obvious emergence of this peak, we can use GOS to partition recrystallized grains from non-recrystallized grains. In this study, we define recrystallized grains as those with a GOS between 0.10° and 0.65°, containing more than 7 scan points (1.52 μm^2), and a confidence index (CI) of greater than 0.05. An example of the use of such partitioning is shown in Figure 3.

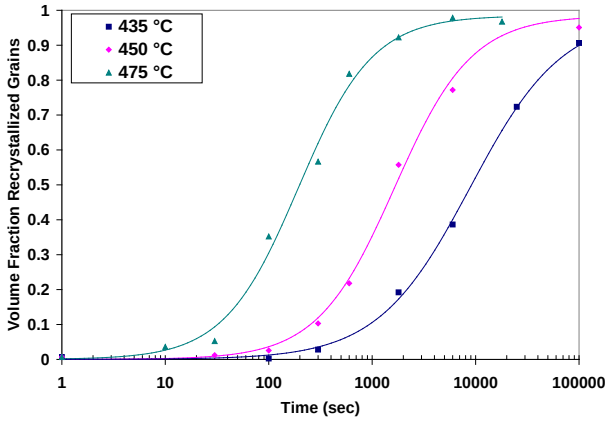

Figure 3. Recrystallized fraction as a function of isothermal annealing temperature and time.

Another observation from Figure2a is that, as recrystallization proceeds, the volume fraction of grains with the highest GOS values decreases such that there are very few grains with high GOS values once recrystallization has proceeded sufficiently. This is consistent with high internal misorientations resulting in a high driving force for recrystallization.

A similar observation can be made based on local misorientation

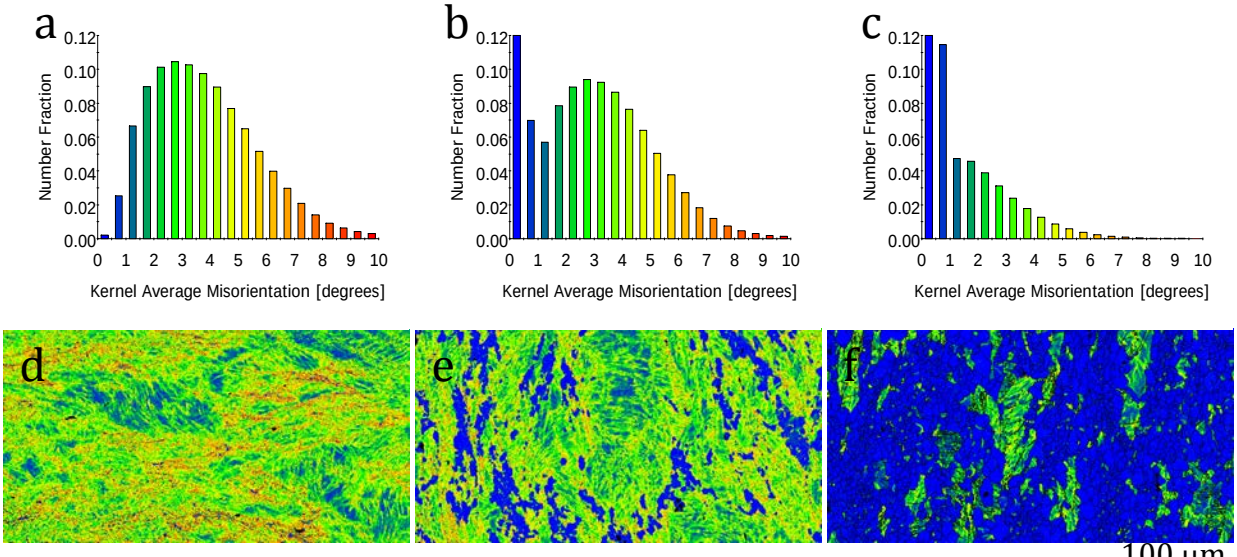

Figure 4. Kernel Average Misorientation (KAM) a-c) scan point distributions and d-f) spatial distributions for isothermal annealing at 450°C for 30 s (a and d), 600 s (b and e), and 6000 s (c

distributions. Figures 4a-c show the evolving distributions of Kernel Average Misorientation (KAM) and Figures 4d-f show the spatial distribution of scan points based on these KAM distributions for different annealing times at 450°C. KAM is based on a local misorientation measure between a scan point and other scan points within a defined kernel. The size of the kernel is defined based on the n^{th} nearest scan point neighbors, and the KAM calculation can include only points at the perimeter of the kernel or all points within the kernel. In addition, misorientations greater than a cut-off value are ignored in the calculation in order to eliminate kernel points lying in neighboring grains. In Figure 4, the KAM calculation is based on the perimeter of a kernel including 3^{rd} nearest neighbors based on a hexagonal scan grid with a cutoff misorientation of 10°. Choosing different kernel sizes (1-10) and cutoff misorientations (5-15°) results in shifts in these distributions, but similar trends. Like the GOS trends, there is a decrease in fraction of individual scan points with higher KAM values with annealing time. Higher values of KAM have been shown to correlate directly with higher geometrically necessary dislocation (GND) densities [20-22], and the prevalent recrystallization of regions of higher KAM earlier in the recrystallization process is also consistent with theories suggesting dislocation content is the driving force for recrystallization.

Figure 5 represents the evolution of crystallographic texture with recrystallization. Figure 5a is an orientation density function (ODF) representation of the texture for the material annealed for 30 s at 450°C that has a recrystallized fraction of less than 1%. Figure 5e is the ODF representation of the texture for the material annealed for 10^5 s at 450°C and has a recrystallized fraction greater than

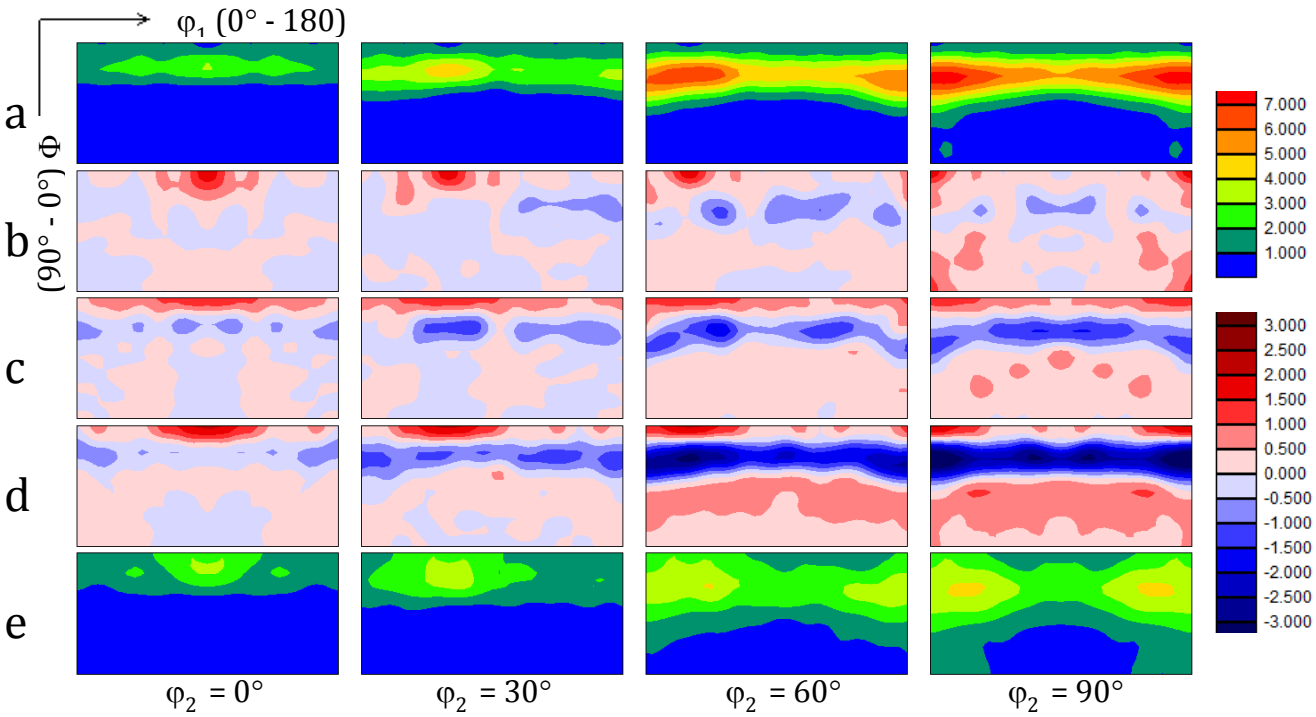

Figure 5. a) Orientation density function (ODF) for isothermal annealing at 450°C for 30 s. ODF difference plots (ODF – ODF(30sec)) for isothermal annealing at 450°C for b) 300 s, c) 1800 s, and c) 10^5 s. e) (ODF) for isothermal annealing at 450°C for 10^5 s.

90%. Figures 5b-5d are ODF difference plots for increasing annealing times at 450°C (300, 1800, and 10^5 s). The ODF difference is calculated by subtracting the ODF calculated at time = 30 s from the ODF calculated for the given annealing time, and thus, represents the change in texture during recrystallization. The ODFs in each case are based on the large step size scans of the entire sample surfaces, are calculated based on spherical harmonics, and assume orthotropic sample symmetry. We observe considerable evolution in texture with recrystallization in this material with a general weakening of initially strong components but without development of strong components that were not strong in the initial material. This result is in contrast to behavior of some FCC metals that exhibit significant strengthening of components that are not strong in the initial deformed microstructure [1, 9, 19], but

similar to behavior observed for HCP alloys during certain recrystallization conditions [12-15].

Discussion

If all points in the deformed microstructure are equally likely to become recrystallized grain nuclei, and there is no favored growth, then the textures before and after recrystallization should match well. The observed differences in the textures and grain sizes before and after recrystallization indicate that certain features of the microstructure influence either the nucleation or growth of recrystallized grains. Based on prior work, many correlations between the deformed microstructure and the resulting recrystallized microstructure can be anticipated. First, the driving force for recrystallization is expected to be higher in grains (or regions) of high dislocation content, which in turn correlates with large values of intra-granular misorientation, such as measured by KAM. Second, it is generally presumed that recrystallization nuclei already exist in the deformed microstructure. Since it is further assumed that recrystallization occurs through the motion of high angle grain boundaries, such recrystallization nuclei are expected to be in close proximity to the high angle boundaries in the deformed microstructure. With further analysis of the EBSD data reported thus far, we seek evidence on whether the above correlations apply to deformed uranium. To do so, we compare the microstructure characteristics of the recrystallized and non-recrystallized microstructures.

We first examine whether grain orientation has an impact on the development of dislocation density. Previous modeling of the deformation behavior

of polycrystalline uranium suggests that some grain orientations tend to accumulate more dislocation density than others [3-6]. The dependence can be partly attributed to the fact that deformation twinning is highly dependent on grain orientation. In suitably oriented grains, twinning can accommodate a significant fraction of the plastic deformation thereby limiting the activity of dislocation slip. In our experimental analysis, as before, we correlate the accumulated dislocation density with the internal misorientation (i.e. KAM). Figure 6 shows different subsets of data from the microstructure of the sample annealed for 30 s at 450°C. Figure 6a shows the KAM number fraction distribution and Figure 6b shows the spatial distribution of scan points with KAM values in different ranges. The blue data have KAM values between 4.95 and 10 representing the top 25% of KAM values, the green data have KAM values between 0 and 2.33 representing the bottom 25% of KAM values, and the red data have KAM values between 2.33 and 4.95 representing the middle 50% of KAM values. Figure 6c is the ODF for all of the data in Figure 6b, Figure 6d is the ODF for the blue data points (highest 25% KAM), and Figure 6e is the ODF for the green data points (lowest 25% KAM). Because these are based on relatively small sets of data, we use discrete binning with a 5° bin size and 5° Gaussian smoothing to calculate the ODFs. Figure 6c differs from Figure 5a in that Figure 5a is based on scans of a large area of the sample (around 7 mm^2) and Figure 6c is from a relatively small area (0.18 mm^2) necessary to calculate spatially resolved orientation statistics such as KAM. We observe considerable differences in the ODFs for the top 25% KAM and bottom 25% KAM. Analysis of ODFs of the non-recrystallized grains in the 100 s sample (not shown) also reveals differences

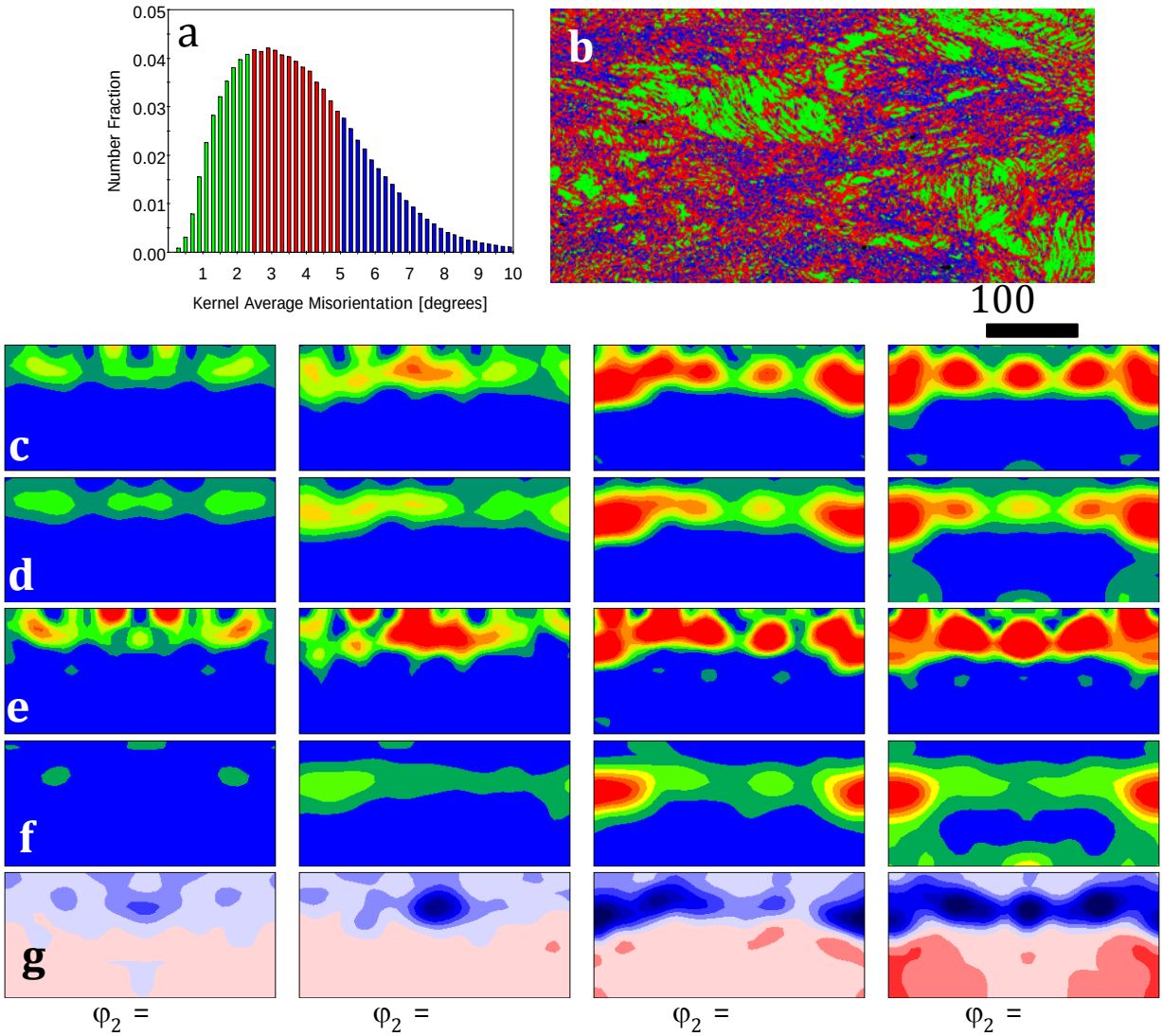

Figure 6. a) KAM distribution for deformed uranium separated by number fractions 0-25%, 25-75%, and 75-100%. b) Spatial distribution of KAM values. c) ODF based on all scan points in b). d) ODF for scan points with 4.95° < KAM < 10°, 75-100%. e) ODF for scan points with 0° < KAM < 2.33°, 0-25%. f) ODF based on scan points along high angle grain boundaries. g) ODF difference based on f minus c. See Fig. 5 for ODF scales

between the highest KAM and lowest KAM orientations. These results clearly indicate a KAM dependence on orientation.

Having revealed an orientation dependence of KAM, we further seek to determine whether grains (or regions) with higher KAM tend to recrystallize earlier. The evolving texture should reflect a possible orientation dependence on

recrystallization. Interestingly, in comparing the ODFs in Figure 6 to the ODF difference plots in Figure 5, no such dependence is seen. The largest ODF differences do not correlate well with either Figure 6d or Figure 6e. Thus it appears the differences in KAM for different orientations are not driving the observed texture evolution. Similarly, for the non-recrystallized grains in the 100 s sample, no clear relation between these ODFs and the ODF difference plots exist. Evidently, while regions of higher local misorientation are recrystallizing earlier in the process, the changes in local orientations are not sufficiently prevalent to have a major effect on the evolving bulk texture.

In light of the foregoing results, next we examine whether recrystallization is preferred at the high angle grain boundary regions. If recrystallization nuclei are in close proximity to high angle boundaries in the deformed microstructure, a difference in orientations in the proximity of grain boundaries relative to the bulk texture may reflect a change in texture during recrystallization. For this analysis, 10° was used to define high angle boundaries. It is apparent from our microstructural datasets that twin boundaries do not act as preferred nucleation sites for recrystallization, and twin boundaries (using a 5° tolerance on the ideal twin boundary misorientation) are thus ignored when considering high angle boundaries. Figure 6f shows the ODF based on the subset of data consisting of EBSD scan points adjacent to high angle grain boundaries, and Figure 6g is the ODF difference between this ODF and the ODF in Figure 6c. The corresponding scan data is shown in Figure 7a. The qualitative similarities between Figure 6g and Figure 5d indicate that the orientation of data points in close proximity to high angle grain

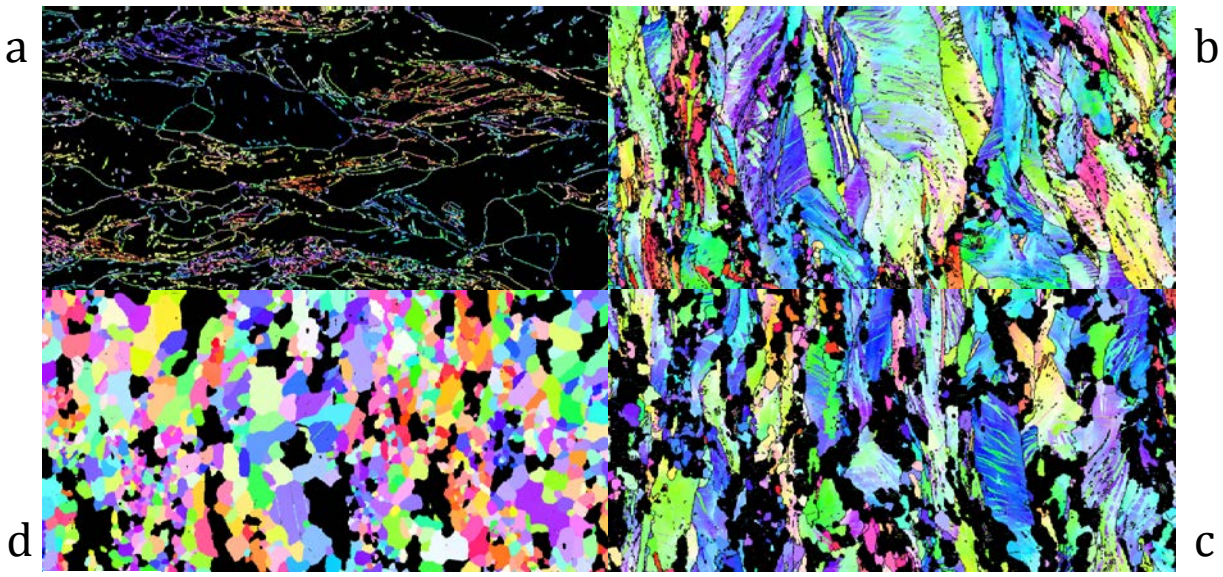

Figure 7. a) heterogeneous distribution of scan points along high angle boundaries for 30 s. Non-recrystallized regions for b) 600 s and c) 1800 s. Recrystallized regions are black and are heterogeneously distributed. d) Recrystallized regions at 10^5 s exhibiting clusters of large grains and clusters of small grains.

boundaries is a good predictor of the recrystallized texture. This indicates that recrystallizing grains tend to nucleate in the vicinity of high angle grain boundaries and grow into neighboring grains, consistent with previous recrystallization studies [1, 9].

To give some insight into recrystallized grain sizes and morphologies, we analyze the evolving microstructures at various stages of recrystallization annealing for 300, 1800, and 10^5 s at 450°C. Figure 7 shows some important features of this evolution. In each figure the orientation of the crystalline direction in the A2 direction is represented (A2 is a consistent in-plane direction in the clock-rolled plate). To locate the potential recrystallization nucleation sites, we analyze the scan points along high angle boundaries, which are given in Figure 7a, used to generate the ODF in Figure 6f. The data reveal that the high angle grain boundaries are not

uniformly distributed throughout the microstructure. Some of the high angle boundaries in the deformed microstructure existed in the material prior to rolling. The density (area per volume) of these boundaries increases with rolling due to the changing shape of the original grains from equiaxed to more pancake shaped [9]. For 50% reduction, this grain shape evolution results in a nominal increase in boundary density. Other, new high angle boundaries develop between the original grain boundaries during deformation. These high angle grain boundaries are caused by accumulation of slip in grains [18, 23-26] or by interactions of twins of different modes or variants. Both of these are likely represented in the microstructure of Figure 7a although it is currently unknown if twin/twin interaction boundaries represent high mobility boundaries. Areas with higher densities of high angle grain boundaries are expected to have more potential recrystallization nucleation sites.

To reveal a possible relationship between recrystallization and high angle grain boundaries, we analyze only the non-recrystallized regions of the microstructure after isothermal annealing at 450°C for 600 and 1800 s, which are displayed Figures 7b and 7c, respectively. High angle grain boundaries are also displayed in these figures and the recrystallized grains are black. These data indicate that recrystallization is not homogeneous within the microstructure with the recrystallized grains existing almost exclusively at the high angle grain boundaries that are not homogeneously distributed within the microstructure.

Another interesting result is found in Fig. 7b. As shown, the most prevalent twin in the deformed microstructure is the {130} twin. The data indicate that recrystallization nuclei are, by and large, not associated with these boundaries.

Last, we analyze in Figure 7d only the recrystallized regions of the microstructure after isothermal annealing at 450°C for 10^5 s. We observe a log-normal distribution of recrystallized grain sizes. However, there are clearly clusters of larger grains and clusters of smaller grains. This heterogeneity is also consistent with the non-homogeneous distribution of high angle grain boundaries and, thus, potential recrystallization nucleation sites. Once a recrystallized grain nucleates, the high angle boundaries between the recrystallization nucleus and deformed regions migrate into the deformed regions until there is no longer a driving force for boundary motion. There will no longer be a driving force for recrystallization boundary motion once the boundary encounters another recrystallized grain (there are still driving forces related to grain coarsening). The local recrystallized grain size is thus dependent on the density of recrystallization nucleation sites that is dependent on the local high angle grain boundary density. Accordingly, in regions where there is a higher density of high angle grain boundaries, the mean free path of the migrating grain boundaries is shorter, and the resulting recrystallized grain size is smaller. In contrast, in regions where there is a low density of high-angle grain boundaries, the mean free path of a moving recrystallization boundary will be larger, and the size of the recrystallized grain will be larger. In the extreme case of regions comprised of only high angle, original boundaries, recrystallizing grains are expected to traverse around half of the original grain before encountering a

recrystallizing grain impinging from the other side, resulting in recrystallized grains with dimensions of around half of the original grain size. In qualitative agreement, we find that the sizes of the larger grains in Figure 7d are about half of the size across the larger regions of low density high angle grain boundaries in Figure 7a.

Conclusions

In this work, we examine how the microstructural characteristics of recrystallizing uranium depend on microstructural characteristics of the deformed uranium using electron backscatter diffraction (EBSD). Relative to the deformed texture, the recrystallization texture is considerably weakened, and occurs without development of strong components that were not strong in the deformed material, which is in contrast to the behavior of many FCC metals but similar to the behavior of HCP metals under certain recrystallization conditions. The data strongly support the notion that recrystallization nucleation occurs along high angle grain boundaries in the deformed microstructure. There is no compelling evidence that either favored nucleation or favored growth has a significant effect on the recrystallization microstructure. The recrystallization texture is similar, but considerably weaker, than the deformation texture, and the texture of points along high angle grain boundaries in the deformed material is a good match for the recrystallization texture. In addition, while there is an orientation dependence on local misorientation, this dependence does not significantly affect the recrystallization texture. The distribution of high angle grain boundaries is inhomogeneous within the microstructure, and nucleation of recrystallized grains correlates well with the spatial distribution of high angle boundaries. This inhomogeneous distribution of

high angle boundaries causes clustered distributions of small and large grains. Twin boundaries do not appear to act as recrystallization nucleation sites.

Acknowledgements

This work is supported by the Los Alamos National Laboratory Directed Research and Development (LDRD) project 20140630ER. Los Alamos National Laboratory is operated by Los Alamos National Security LLC under DOE Contract DE-AC52-06NA25396. Electron microscopy was performed at the Los Alamos Electron Microscopy Laboratory.

Bibliography

1. R. D. Doherty, D. A. Hughes, F. J. Humphreys, J. J. Jonas, D. J. Jensen, M. E. Kassner, W. E. King, T. R. McNelley, H. J. McQueen,A. D. Rollett, Mat. Sci. Eng. A-Struct. 238 (1997) 219-274.
2. D. W. Brown, M. A. M. Bourke, B. Clausen, D. R. Korzekwa, R. C. Korzekwa, R. J. McCabe, T. A. Sisneros,D. F. Teter, Mat. Sci. Eng. A-Struct. 512 (2009) 67-75.
3. R. J. McCabe, L. Capolungo, P. E. Marshall, C. M. Cady,C. N. Tome, Acta Mater. 58 (2010) 5447-5459.
4. M. Knezevic, L. Capolungo, C. N. Tome, R. A. Lebensohn, D. J. Alexander, B. Mihaila,R. J. McCabe, Acta Mater. 60 (2012) 702-715.
5. M. Knezevic, R. J. McCabe, R. A. Lebensohn, C. N. Tome, C. Liu, M. L. Lovato,B. Mihaila, J. Mech. Phys. Solids 61 (2013) 2034-2046.
6. M. Knezevic, R. J. McCabe, C. N. Tome, R. A. Lebensohn, S. R. Chen, C. M. Cady, G. T. Gray, III,B. Mihaila, Int. J. Plasticity 43 (2013) 70-84.
7. R. J. McCabe,D. F. Teter, J. Microsc.-Oxford 223 (2006) 33-9.
8. R. D. Doherty, Recrystallization of Metallic Materials. Dr. Rieder Verlag: Berlin, 1978.
9. F. J. Humphreys,M. Hatherly, Recrystallization and Related Annealing Phenomena. Pergamon Press: Oxford, 1995.
10. R. D. Doherty, Prog. Mater. Sci. 42 (1997) 39-58.
11. A. D. Rollett, Prog. Mater. Sci. 42 (1997) 79-99.
12. F. Wagner, N. Bozzolo, O. Van Landuyt,T. Grosdidier, Acta Mater. 50 (2002) 1245-1259.

13. F. Gerspach, N. Bozzolo,F. Wagner, Scripta Mater. 60 (2009) 203-206.
14. B. Bacroix, J. Tarasiuk, K. Wierzbanowski,K. Zhu, Journal of Applied Crystallography 43 (2010) 134-139.
15. K. Y. Zhu, D. Chaubet, B. Bacroix,F. Brisset, Acta Mater. 53 (2005) 5131-5140.
16. D. G. Brandon, Acta Metall. 14 (1966) 1479-&.
17. D. M. Saylor, B. S. El-Dasher, B. L. Adams,G. S. Rohrer, Metall. Mater. Trans. A 35A (2004) 1981-1989.
18. S. Wang, E. A. Holm, J. Suni, M. H. Alvi, P. N. Kalu,A. D. Rollett, Acta Mater. 59 (2011) 3872-3882.
19. M. H. Alvi, S. W. Cheong, J. P. Suni, H. Weiland,A. D. Rollett, Acta Mater. 56 (2008) 3098-3108.
20. D. P. Field, P. B. Trivedi, S. I. Wright,M. Kumar, Ultramicroscopy 103 (2005) 33-39.
21. W. Pantleon, Scripta Mater. 58 (2008) 994-997.
22. B. S. El-Dasher, B. L. Adams,A. D. Rollett, Scripta Mater. 48 (2003) 141-145.
23. C. N. Tome, R. A. Lebensohn,C. T. Necker, Metall. Mater. Trans. A 33 (2002) 2635-2648.
24. B. Bay, N. Hansen, D. A. Hughes,D. Kuhlmannwilsdorf, Acta Metall. Mater. 40 (1992) 205-219.
25. D. A. Hughes, Q. Liu, D. C. Chrzan,N. Hansen, Acta Mater. 45 (1997) 105-112.
26. Q. Xue, I. J. Beyerlein, D. J. Alexander,G. T. Gray, III, Acta Mater. 55 (2007) 655-668.